https://doi.org/10.1016/j.est.2020.101421

Performance optimization for shell-and-tube PCM thermal energy storage

Haobin Liang[1], Jianlei Niu*[1, 2], Yixiang Gan[1]

1. School of Civil Engineering, The University of Sydney
2. Department of Building Services Engineering, The Hong Kong Polytechnic University

*Email of corresponding author: jian-lei.niu@polyu.edu.hk

Highlights

- To optimize LHTES units, an index E_{st} based on effectiveness-NTU theory, was adopted.
- E_{st} captures effects from geometric arrangements and leads to an optimal PCM volume ratio.
- Increasing k_{eff} is only effective in enhancing E_{st} when PCM volume ratio is above a certain value.
- The peak E_{st} of fully turbulent flows are generally lower than those of laminar flows.
- The method is recommended as a standard one in designing a shell-and-tube LHTES system.

Abstract

Phase change material (PCM) based latent heat thermal energy storage (LHTES) systems have been a technology of increasing interests. Extensive experimental and numerical studies on the heat transfer enhancement of PCM have been reported. However, a thorough analysis of the effects of PCM heat transfer enhancement in combination with geometric optimization on the overall storage performance of an LHTES system is still lacking. In this work, a performance index, the effective energy storage ratio E_{st}, based on the effectiveness-NTU theory, which set up a standard to compare TES systems, was adopted to evaluate the effective energy storage density of an LHTES system. Using the conjugate heat transfer analysis, we investigated the impact of the key parameters and flow conditions, including the geometric parameters (tube length-diameter ratio L/d_i, PCM volume ratio λ), turbulent versus laminar flow conditions of HTF, and the effective PCM thermal conductivity k_{eff}, on the performance indicator E_{st}. It was found that the effective energy storage ratio increases with tube length-diameter ratio, and an optimal PCM volume ratio exists. Increasing the effective PCM thermal conductivity is only effective in enhancing the

effective energy storage ratio when PCM volume ratio is above certain value. Over 500 sets of parametric studies were performed to optimize the PCM volume by maximizing the effective energy storage ratio. The results show that for both laminar and turbulent flow, optimal PCM volume ratio and maximal effective energy storage ratio increases with tube length-diameter ratio and effective PCM thermal conductivity. The enhancement of effective PCM thermal conductivity only noticeably increases maximal effective energy storage ratio when tube length-diameter ratio is above a certain threshold, i.e., around 800 for laminar flow and around 600 for fully turbulent flow. The fully turbulent flow greatly enhances the charging rate by 50 times and increases the capacity effectiveness at optimal PCM volume ratio to 0.6-0.9 from 0.2-0.8 at laminar flow conditions, but the maximal effective energy storage ratio of fully turbulent flows are generally lower than those of laminar flows. This work is the first systematic numerical analysis of the complete ensemble design factors of a shell-and-tube LHTES system, and it is recommended that the method could be a standard one for the engineering design of an LHTES system.

Keywords: Phase change material; Design optimization; Latent heat thermal energy storage; Shell-and-tube; Effective energy storage ratio

Nomenclature

c_p specific heat capacity, $\mathrm{kJ/(kg \cdot K)}$
d tube diameter, m
ΔT temperature range of phase change, K
E_{st} effective energy storage ratio, -
$E_{st,op}$ maximal effective energy storage ratio, -
h specific enthalpy, $\mathrm{kJ/kg}$
k thermal conductivity, $\mathrm{W/(m \cdot K)}$
L tube length, m
L/d_i tube length-diameter ratio, -
H latent heat, $\mathrm{kJ/kg}$
$\dot{m}$ mass flow rate, $\mathrm{kg/s}$
q_c charging rate, W
Q_{eff} effective energy storage capacity, J
Q_∞ theoretical energy storage capacity, J
r radial distance, m
t time, s
T temperature, K
u axial velocity, $\mathrm{m/s}$
V, volume, $\mathrm{m^3}$
$\dot{V}$, volume flow rate, $\mathrm{m^3/s}$
$\boldsymbol{v}$ velocity vector, $\mathrm{m/s}$

Subscripts
eff effective
i inner tube
in inlet
l liquid
m melting
o outer tube
op optimal
out outlet
p pump
s solid
w water

Greek letters
ρ density, $\mathrm{kg/m^3}$
η heat transfer effectiveness, -
λ PCM volume ratio, -
μ dynamic viscosity, $\mathrm{Pa \cdot s}$
φ capacity effectiveness, -

Abbreviations
HTF heat transfer fluid
LHTES latent heat thermal energy storage
NTU number of heat transfer unit
PCM phase change material
SWS stratified water storage
TES thermal energy storage

1 Introduction

As global energy faces the challenge of more energy demands and less carbon emission, the proportion of renewable energy is increasing in recent years, which raises higher requirement on the stability of the system operation [1, 2]. By shifting load between on-peak and off-peak hours, thermal energy systems (TES) can mitigate the mismatch between energy supply and demand [3]. Furthermore, intermittent energy supply issues could be solved with the application of TES. Due to the large latent heat released or absorbed during the phase change process, phase change materials (PCM) are gaining wide attention over the past years. Compared with traditional thermal energy storage (TES) system making use of the sensible heat, latent heat thermal energy storage (LHTES) using PCM can normally provide higher energy storage capacity and efficiency [3].

In order to improve the feasibility of LHTES systems, extensive studies focus on enhancing the heat transfer in PCM to achieve a higher effective thermal conductivity. Even though the high thermal storage density of PCM is beneficial to improve LHTES performance, the low thermal conductivity of PCM, normally around 0.2-0.5$\mathrm{W/(m \cdot K)}$ [4], remains as an issue, which could lead to the inefficiency of the large-scale practical utilization [5]. By combining materials of high thermal conductivity with PCMs or encapsulating PCMs, the heat transfer performance can be notably enhanced. Graphite matrices [6], carbon-based fillers [7-9] (eg. carbon fiber, nano-graphite (NG), multi-walled carbon nanotubes (MWCNTs) and graphene nanoplatelets), metal foams [10-12] can improve the effective thermal conductivity of pure PCM from 20 times to 150 times and enhance the phase change rate significantly, depending on the materials used and their fractions. Furthermore, microencapsulating PCM with zirconia shell could increase the effective thermal conductivity by 6 times [13], installing fins can reduce the solidification time up to 43.6% [14] and corrugated fins could reduce the total solidification time by 30–35% compared with flat fins [15]. The interest in combining nanoparticles and fins for applications is growing in recent years [16, 17].

More than 70% of studies on LHTES systems focus on the shell-and-tube type, due to its pipe geometry and minimal heat loss [18]. The cylindrical shell-and-tube unit has shown its advantages in terms of the heat transfer rate, under the same conditions. Esen et al. [19] applied four types of PCM and compared the cylinder model and pipe model for cylindrical latent heat storage tanks by developing a theoretical model. They found out that the pipe model of fluid embedded in the bulk PCM, showed a much shorter melting time. Vyshak et al. [20] numerically compared different containers with calcium chloride hexahydrate as PCM. They concluded that cylindrical shell containers take the least time under the same energy storage volume and surface area, compared with the rectangular and cylindrical configuration. The effects of different design parameters on a shell-and-tube TES unit including orientation, the properties of heat transfer fluid (HTF) and PCM have been widely studied. Akgün et al. [21] experimentally evaluated the effect of the tilting angle on the cylindrical shell LHTES container using paraffin. It was noticed that with an inclination angle of 5 degrees, the total melting time decreased by approximately 30%. Seddegh et al. [22] performed a comparative numerical study on the shell-and-tube system. It was found that the horizontal orientation showed a higher charging rate than vertical orientation, but no obvious difference was shown for the discharging process. Li et al. [23] numerically investigated the melting process of the multiple PCM system filled with three types of molten salt and fully developed turbulent air flow was adopted as HTF. The optimal lengths for each PCM and air inlet temperature were found. The influences of the HTF mass flow rate and inlet temperature [20-26] on the phase change process are extensively researched.

Furthermore, the energy storage performance of the shell-and-tube LHTES units or

systems and optimizations have been investigated. Charging and discharging time [19-21, 26] are the most widely used to measure energy storage efficiency. Esen et al. [19] numerically performed an optimal geometric design for four different types of PCM, based on the index of whole PCM melting time. Wang et al. [27] proposed the energy efficiency ratio in the shell-and-tube system, which is defined as the heat energy stored per unit mechanical energy consumption during the operation. It was revealed that the ratio is more sensitive to the outer tube diameter and decreases with the increase of tube length and outer tube diameter. Fang et al. [28] defined a new index of effective energy storage ratio to characterize the energy storage capacity of the LHTES system, which is the ratio of the stored heat over that of an ideal stratified water storage (SWS) tank of the same volume. It is proposed to be the objective of the design optimization of an LHTES system. In an ensuing analytical study based on the NTU-effectiveness theory [29], Fang et al. revealed the impacts of operating parameters of laminar versus turbulence of the heat transfer fluid on the shell-and-tube LHTES systems. Amin et al. [25] defined the energy storage density coefficient α for the slab type LHTES system, which considers both the charging and discharging process, and an optimal plate thickness was found under different flow rates to maximize the coefficient. In addition, increasing the gap thickness and mass flow rate would decrease the coefficient. Qarnia [30] studied the thermal performance of a solar latent heat storage unit and the optimal tube number was found for three types of PCM, by measuring the thermal storage efficiency under the given summer climate in Marrakech city. Talmatsky and Kribus [31] performed an annual simulation for domestic solar water heating systems with MATLAB and TRYSYS. Through comparison with systems without PCM, they pointed out that the application of PCM does not yield a significant benefit. It is worthwhile to mention that their results show that a proper design of the geometry of LHTES systems is crucial to make the envisioned potential of PCM come true.

Despite extensive experimental and numerical studies on heat transfer enhancement of PCM and the qualitative effects of heat transfer fluid (HTF) properties in LHTES systems, no systematic numerical analysis of the complete ensemble design factors of a shell-and-tube LHTES system has been proposed. A thorough analysis of the geometric impacts on energy storage performance is crucial to the system design in applications, especially when other conditions are varying.

The goal of the research is to find out the optimal PCM volume ratio λ_{op}, under different tube length-diameter ratios L/d_{i}, effective thermal conductivities of PCM k_{eff} and HTF flow conditions (laminar vs turbulent), which could serve as guidance when designing shell-and-tube TES systems using PCM. The performance index, effective energy storage ratio E_{st}, based on the effectiveness-NTU theory and proposed by Fang [28], was adopted in this study as the maximization goal. Under specified L/d_i and k_{eff}, optimal PCM volume ratios λ_{op} were found through over 500 sets of parametric studies in the numerical simulation. Optimal PCM volume ratios and maximal effective energy storage ratios $E_{st,op}$ were compared under laminar and

turbulent flow conditions. It is recommended that the method be a standard one for the engineering design of an LHTES system.

2 Methodology

2.1 System characterization

A single concentric cylinder unit from a shell-and-tube type LHTES system was selected as the geometry for the numerical simulation in this study. As shown in Fig. 1, the 3D domain was simplified into the 2D axisymmetric domain in the simulation.

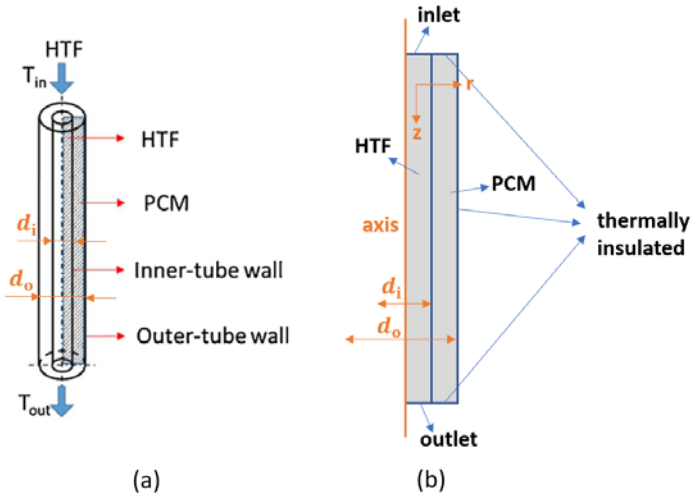

Fig. 1. (a) 3D shell-and-tube concentric cylinder unit;
(b) 2D axisymmetric simplification

Based on the specified geometry, the index of effective energy storage ratio E_{st} [28] for the melting process of PCM is defined as:

$$E_{st} = \frac{Q_{\text{eff}}}{Q_{SWS}} \tag{1}$$

$$Q_{SWS} = \rho_w c_{p,w} V (T_{in} - T_0) \tag{2}$$

$$Q_{\text{eff}} = \int_0^{t_{\text{eff}}} \dot{m}\, c_{p,w} (T_{in} - T_{out}) dt \tag{3}$$

where Q_{eff} is the effective energy storage capacity of the LHTES system, evaluating the actual amount of the heat stored by the energy storage unit during the melting process. Q_{SWS} is the effective energy storage capacity of an ideal stratified water storage (SWS) system. T_0 is the initial temperature and V refers to the volume of the SWS system. T_{out} is calculated as the mass-weighted average temperature over

the outlet surface:

$$T_{out} = \frac{\int_0^{\frac{d_i}{2}} T(r) \cdot \rho_w u(r) \cdot 2\pi r dr}{\dot{m}} = \frac{\int_0^{\frac{d_i}{2}} T(r) u(r) r dr}{\int_0^{\frac{d_i}{2}} u(r) r dr} \quad (4)$$

The effective energy storage capacity Q_{eff} is calculated before the outlet temperature T_{out} reaches a specified value. The specified value of T_{out} is determined by the heat transfer effectiveness η, which is based on the effectiveness-NTU theory.

The effectiveness-NTU theory has been applied to investigate the performance of the LHTES system [25, 29, 32, 33]. The studies describe a TES system using phase change materials as a heat exchanger, in which PCM exchanges heat with the heat transfer fluid at the phase change temperature (i.e. melting temperature T_m in this study) [32]. Therefore, the heat transfer effectiveness for the melting process is defined as:

$$\eta = \frac{T_{in} - T_{out}}{T_{in} - T_m} = 1 - e^{-NTU} \quad (5)$$

The heat transfer effectiveness η describes the relationship of the actual heat transferred and the theoretical maximum heat could be transferred. The effect of the sensible energy absorbed or released is small compared with the latent heat energy. Thus, the sensible energy of the PCM is ignored in the definition of η.

According to the equation defined, maximum heat transfer effectiveness $\eta = 1$ is achieved when the outlet temperature equals the melting temperature of PCM $T_{out} = T_m$. As the outlet temperature T_{out} increases when PCM is melting, the heat transfer effectiveness η decreases. In order to ensure the heat transfer effectiveness of the PCM storage system, a minimum value of η should be considered for design optimization. Afterward, the specified outlet temperature T_{out} and the value of t_{eff} could be determined to calculate the effective energy storage capacity Q_{eff}. In this study, $\eta = 0.8$ was chosen as the minimum heat transfer effectiveness for the shell-and-tube TES unit. In typical building cooling and heating applications, the time scale of the charging and discharging will be typically a few hours on daily basis. To maximize the utilization of peak solar radiation and night time cooling, it is also desirable that speedy charging can be realized as for electric cars. Therefore, the time scale required to complete the charging is a very important performance indicator of a PCM storage device. In this study the time required to reach the specified temperature is used as the cut-off time to define the effective energy storage ratio E_{st}.

For the reference purpose, the capacity effectiveness φ and the theoretical energy storage capacity Q_∞ are defined as:

$$\varphi = \frac{Q_{\text{eff}}}{Q_\infty} \quad (6)$$

$$Q_\infty = \lambda \rho_{PCM} V [c_{p,PCM}(T_{in} - T_0) + H] + (1 - \lambda) \rho_w c_{p,w} V (T_{in} - T_0) \quad (7)$$

where V is the volume of the LHTES system and λ is the PCM volume ratio, which is defined as the ratio of PCM volume and the LHTES system volume:

$$\lambda = \frac{V_{PCM}}{V} = 1 - \frac{{d_i}^2}{{d_o}^2} \quad (8)$$

To measure the energy storage efficiency in terms of time, the charging rate q_c is defined as:

$$q_c = \frac{Q_{\text{eff}}}{t_{\text{eff}}} \quad (9)$$

In conclusion, the LHTES system performance is evaluated by effective energy storage ratio E_{st}. If $E_{st} > 1$, it means that the LHTES system is effective as it shows better energy storage performance than the traditional SWS system. Otherwise, $E_{st} < 1$ means the system is ineffective compared with an SWS system. A higher value of E_{st} means a more effective LHTES system. The goal of the design optimization is to maximize the index E_{st}.

2.2 Numerical model

The commercial modeling software COMSOL Multiphysics 5.3a, based on the finite element method (FEM), is used for the numerical study. The Heat Transfer module and Fluid Flow module are applied for the conjugate heat transfer of the melting process of PCM in the concentric cylindrical shell-and-tube unit. Through the scale analysis, Lorente et al. [34] proposed the theoretical criteria of the critical time when convection becomes dominant as $t_f \sim \left(\frac{L\upsilon}{\alpha g \beta \Delta T}\right)^{1/2}$. In the evolution of the melting front in their paper, the natural convection starts to show its impacts during 500s to 1000s. Consequently, in this study, by assuming the same thermal expansion coefficient for paraffin wax as 0.002K^{-1}, and the tube length as 5m, the time when natural convection begins to exhibit influences is during 3237s~6473s. The simulation time scale of almost all cases is below this time range and higher tube lengths were studied, which results in a higher critical time. In addition, the effect of the natural convection would be hindered by the heat transfer enhancement, e.g. filling metal foam and expanded graphite, and by using folded or spirally shaped long tubes [28]. Therefore, the natural convection effect was ignored in the simulation.

The continuity, momentum and energy equations of the heat transfer fluid (water) are:

$$\rho \nabla \cdot (\boldsymbol{v}) = 0 \quad (10)$$

$$\rho \frac{\partial \boldsymbol{v}}{\partial t} + \rho(\boldsymbol{v} \cdot \nabla)\boldsymbol{v} = \nabla \cdot [-p + \mu(\nabla \boldsymbol{v} + (\nabla \boldsymbol{v})^T)] + \rho g \quad (11)$$

$$\rho c_p \frac{\partial T}{\partial t} + \rho c_p \boldsymbol{v} \cdot \nabla T + \nabla \cdot (-k \nabla T) = 0 \quad (12)$$

As shown in Fig. 1, inlet velocity u_{in}, inlet temperature T_{in} and outlet pressure p_{out} were chosen as the boundary conditions for HTF. No-slip wall condition was applied for the inner tube and the thermal resistance between HTF and PCM was ignored. All other boundaries were assumed as thermally insulated. In applications, there could be heat leakage affecting the latent heat storage performance. However, the dimensionless performance index E_{st} already considers the same properties of HTF and storage unit geometry between latent and sensible heat storage. Therefore, the amount of latent heat leakage would be on the same scale as the heat leakage in the SWS system.

For the PCM domain, the effective heat capacity method is applied as the approach to solving the phase change process. As opposed to the enthalpy method, which calculates the liquid fraction during the phase change process, the effective heat capacity method uses the effective heat capacity of PCM in the governing equation, which is the derivative of the enthalpy and directly proportional to the energy absorbed or released. The approach could reflect the phase change temperature range of PCMs, which is important to obtain more precise results of the LHTES system. The method was firstly proposed by Salcudean and Poirier [35]. Iten et al. [36] compared the enthalpy method and the effective heat capacity method for the simulation of the air-TES horizontal metallic panel unit. The results showed that the effective heat capacity method accurately predicted the smooth increase during the phase change process, while the enthalpy method showed a phase change process more appropriate for pure PCMs.

The governing equation for the PCM domain under the effective heat capacity approach is defined as:

$$\rho c_{p,eff} \frac{\partial T}{\partial t} + \nabla \cdot (-k \nabla T) = 0 \tag{13}$$

The approach assumes that the specific heat of PCM is a function of temperature $c_p = f(T)$. As shown in Fig. 2 (a), the modified step function $\sigma(x)$ is applied to define the effective heat capacity in the phase change region. The size of the transition zone is the phase change temperature range of PCM. Therefore, the enthalpy during the melting process is:

$$h = c_{p,s} T + H \cdot \sigma(T - T_m) \tag{14}$$

$$T_m = \frac{T_s + T_l}{2} \tag{15}$$

where T_m is the melting temperature, T_s and T_l refer to the start temperature and end temperature of the melting process. H is the latent heat of PCM and $c_{p,s}$ is the specific heat capacity for solid PCM. The melting temperature range is $\Delta T = T_l - T_s$. The effective heat capacity reaches the maximum value at the middle point of the melting range, i.e. at the melting temperature T_m.

Therefore, the effective specific heat capacity applied in the governing equation is:

$$c_{p,eff} = \begin{cases} c_{p,s}, & T \le T_s \\ \dfrac{d\mathrm{h}}{dT}, & T_s < T < T_l \\ c_{p,l}, & T \ge T_l \end{cases} \tag{16}$$

Table 1 PCM properties used in this study

Property	Value
Density ($\mathbf{kg/m^3}$)	770
Thermal conductivity ($\mathbf{W/(m \cdot K)}$)	0.14
Specific heat capacity ($\mathbf{kJ/(kg \cdot K)}$)	2.2
Latent heat ($\mathbf{kJ/kg}$)	182.7
Melting temperature (K)	285

The properties of PCM [37] used for parametric studies in this paper are shown in Table 1. According to equation (16), the effective specific heat $c_{p,eff}$ varying with temperature implemented in the software with a temperature range of 2℃ is shown in Fig. 2 (b).

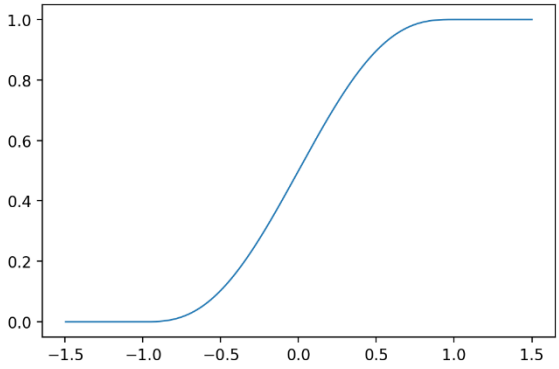

(a) Step function

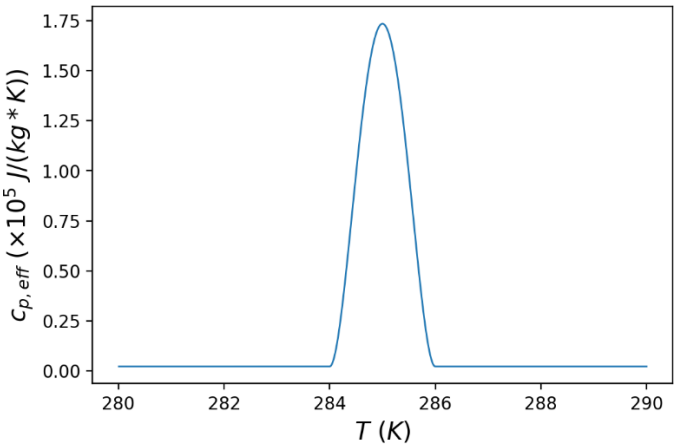

(b) Effective specific heat capacity $c_{p,eff}$

Fig. 2. The effective specific heat method

A time-dependent solver with the segregated method and the direct solver of

PARDISO was applied for the simulation. Implicit BDF (Backward Differentiation Formula) was applied for the time-dependent solver. The absolute tolerance for the solver was set to be 0.0001. In the finite element method, the element order for the discretization refers to the basis functions applied in the simulation. The effect of the element order on numerical results was checked and no significant difference for the temperature results was exhibited between the first and second-order discretization for the fluid flow and heat transfer module. Considering the less memory usage and more efficient computational process, the first-order element was applied to solve the velocity, pressure and temperature field, according to the justified default setting in COMSOL. The mesh sensitivity study will be performed during the validation stage.

To numerically investigate the effective energy storage for the turbulent flow in the LHTES system with PCM, the $k-\varepsilon$ model was applied to study the turbulence effect for the heat transfer fluid. The inlet data for the turbulence variables are approximated for k, ε by the following formulas [38]:

$$k = \frac{3}{2}(|\boldsymbol{U}|I_T)^2 \tag{17}$$

$$\varepsilon = C_\mu^{\frac{3}{4}} \frac{k^{\frac{3}{2}}}{L_T} \tag{18}$$

The turbulence length scale for 2D flows for pipes can be estimated by $L_T = 0.07d_i$. The turbulent intensity I_T was adopted as 10% for the inlet in this work. A time step of 0.01s was set up for turbulent flow. Mesh size was kept the same as the one for laminar flow and mesh independence was checked for turbulent flow.

2.3 Model Validation

The velocity and temperature distributions of heat transfer fluid were validated by the analytical results of steady laminar and turbulent pipe flow. Gravity was and the mesh independence was checked. For laminar flow validation, water was chosen as the heat transfer fluid with property defined as follows: density $\rho = 998.2\mathrm{kg/m^3}$, specific heat capacity $c_p = 4182\mathrm{J/(kg\cdot K)}$, thermal conductivity $k = 0.6\mathrm{W/(m\cdot K)}$, viscosity $\mu = 0.001003\mathrm{kg/(m\cdot s)}$ and inlet velocity $u = 0.005\mathrm{m/s}$. The according Reynolds number and Prandtl number are 995 and 6.99, respectively. The pipe diameter is $0.2\mathrm{m}$ and the pipe length is $100\mathrm{m}$. The outlet boundary condition is atmospheric pressure. The inlet temperature of HTF and wall temperature are $298\mathrm{K}$ and $313\mathrm{K}$. Equations (19) to (22) [39, 40] are applied to validate the entrance length, outlet velocity distribution, pressure in the fully developed region and heat transfer under constant wall temperature.

$$\frac{L_\mathrm{e}}{d} \approx 0.06\mathrm{Re} \tag{19}$$

$$u = \frac{R^2}{4\mu}\left(-\frac{dp}{dx}\right)\left(1 - \frac{r^2}{R^2}\right) \tag{20}$$

$$\Delta p = \frac{8\mu L\dot{V}}{\pi R^4} \tag{21}$$

$$\mathrm{Nu}_d = 3.66 + \frac{0.0668\left(\frac{d}{L}\right)\mathrm{Re}\cdot\mathrm{Pr}}{1 + 0.04\left[\left(\frac{d}{L}\right)\mathrm{Re}\cdot\mathrm{Pr}\right]^{\frac{2}{3}}} \tag{22}$$

Numerical results of COMSOL 5.3a of laminar pipe flow are plotted in Fig. 3. It could be clearly seen that the software gives accurate results, compared with analytical equations and the correlation. According to Eq. (19), the theoretical entrance length for the laminar pipe flow is $11.94\mathrm{m}$. The entrance length obtained from the numerical simulation is $11.40\mathrm{m}$, as shown in Fig. 3 (a), which agrees well with the theoretical value. Moreover, the maximal centerline velocity matches well with theoretical data $u_{\max} = 2u = 0.01\mathrm{m/s}$. The outlet velocity distribution was obtained by calculating the pressure drop over the entire pipe and Fig. 3 (b) shows that numerical results match well with Eq. (20). When the outlet pressure as 0, the relative pressure at other points in the pipe is shown in Fig. 3 (c). In the fully developed region, numerical results show good agreement with the theoretical results in Eq. (21). For numerical studies, the Nusselt number was obtained by calculating the heat transfer coefficient, which is based on the logarithmic temperature difference between wall temperature and mass-weighted average bulk temperature each cross-section. As shown Fig. 3 (d), numerical data agrees well with the heat transfer correlation of laminar pipe flow.

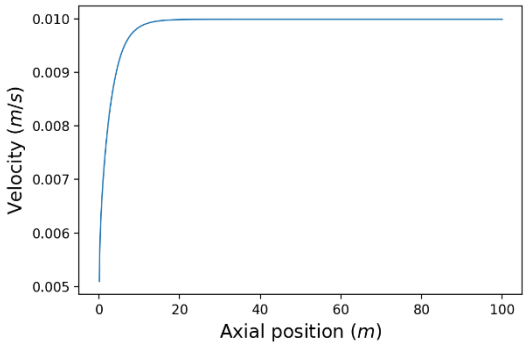

(a) Velocity at the centerline

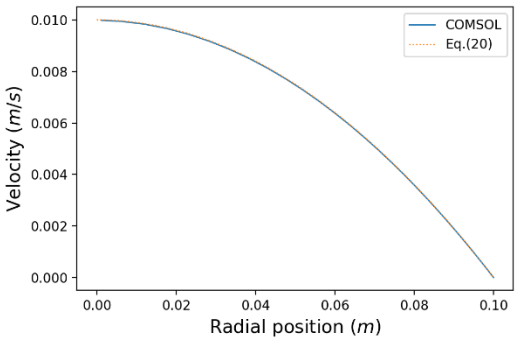

(b) Outlet velocity

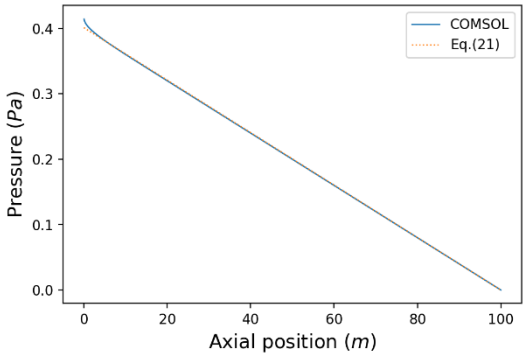

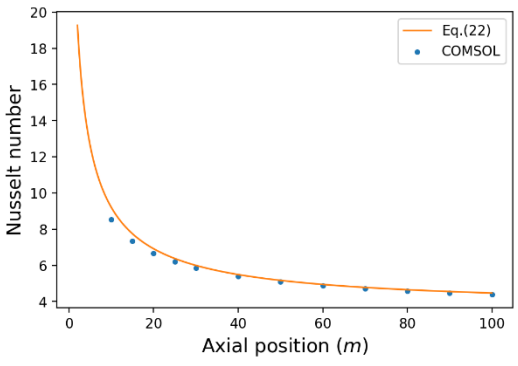

(c) Pressure (d) Nusselt number

Fig. 3. Validation of HTF against analytical laminar pipe flow results

As for turbulent pipe flow validation, except that pipe length is $20\mathrm{m}$ and inlet velocity is $0.0754\mathrm{m/s}$, other parameters are kept the same as those in laminar pipe flow. The according Reynolds number is 15000. Equations (23) to (27) [39, 40] are applied to validate the entrance length and heat transfer in the fully developed region.

$$\frac{L_\mathrm{e}}{d} \approx 4.4\mathrm{Re}^{\frac{1}{6}} \tag{23}$$

$$\frac{V}{u_\mathrm{max}} \approx \left(1 + 1.3\sqrt{f}\right)^{-1} \tag{24}$$

$$\frac{\bar{u}}{u_\mathrm{max}} = \left(1 - \frac{r}{R}\right)^{\frac{1}{n}} \tag{25}$$

$$\Delta p = f\frac{\rho L V^2}{2d} \tag{26}$$

$$\mathrm{Nu}_d = 0.023\mathrm{Re}^{0.8}\mathrm{Pr}^{0.4} \tag{27}$$

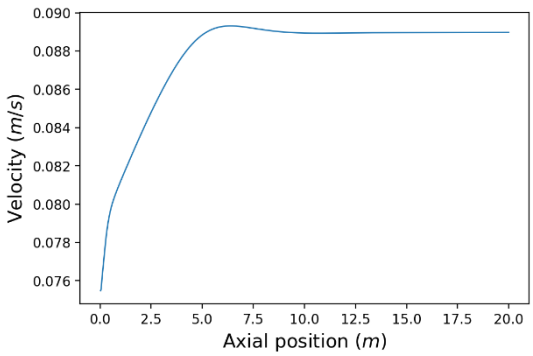

(a) Velocity at the centerline

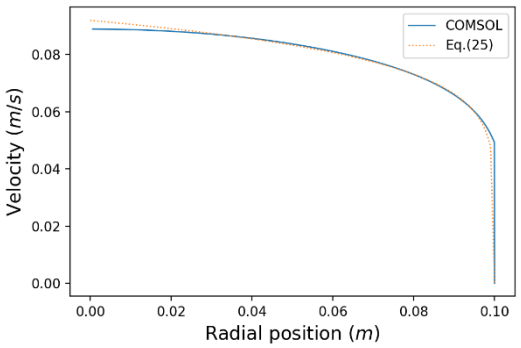

(b) Outlet velocity

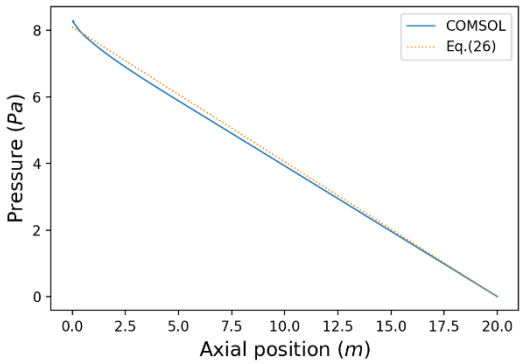

(c) Pressure

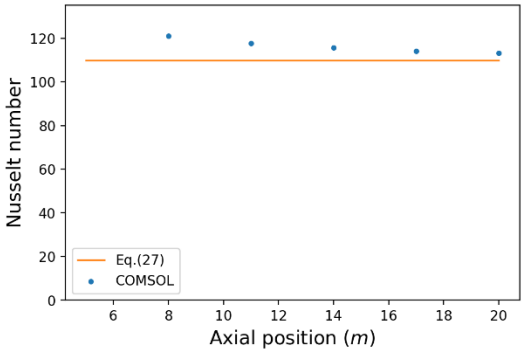

(d) Nusselt number

Fig. 4. Validation of HTF against analytical turbulent pipe flow results

The numerical results of COMSOL 5.3a are compared with experimental correlations. The friction factor is calculated by the Blasius equation for smooth pipes, which is $f =$

$0.316\mathrm{Re}^{-1/4}$. The centerline velocity overshoot appeared in Fig. 4 (a) has been observed in experimental and numerical studies, which is due to a radial inflow of fluid toward the centerline of the pipe followed downstream by a radial outflow from the centerline to the wall[41]. In addition, their results exhibited that the higher inlet turbulence intensity, the lower the magnitude of the overshoot and higher entrance length. This could explain the discrepancy of the entrance length between numerical results shown in Fig. 4 (a) ($6.40\mathrm{m}$) and the theoretical one calculated by Eq. (23) ($4.37\mathrm{m}$). The maximal velocity at the centerline in the fully developed region is close to the one calculated from correlation Eq. (24), i.e., $0.092\mathrm{m/s}$. Fig. 4 (b) and Fig. 4 (c) show that in the fully developed region, the velocity distribution in the radial direction and pressure in the axial direction match well the empirical correlation. Considering that the correlation would underpredict Nusselt number by 7-10 percent when the Prandtl number is higher [42] and a higher inlet turbulence intensity would lead to a higher Nusselt number in the numerical study, the discrepancy, i.e. $e = (113 - 109)/109 \times 100\% \approx 3.7\%$, between numerical results and Eq. (27) within the fully developed region shown in Fig. 4 (d) is acceptable.

The result of the melting process of PCM from Trp's experimental study [43] was applied for model validation. The parameters for the shell-and-tube system and PCM properties used in Trp's work are specified in Table 2.

The melting range of the phase change material RT 30 was given by Trp as $\Delta T = 35 - 27.7℃ = 7.3℃$. In the validation, it was assumed that the maximum effective specific heat appears when the temperature is at the middle point of the melting temperature range. In other words, the melting temperature used as the input for the model is $T_m = T_s + \Delta T/2 = 31.35℃$, and the temperature range is accordingly from $T_m - \Delta T/2$ to $T_m + \Delta T/2$.

Table 2 System parameters and PCM properties for validation

System Parameter	Value
Tube length (m)	1
Inner tube diameter (m)	0.033
Outer tube diameter (m)	0.128
Mass flow rate (kg/s)	0.017
Inlet temperature (℃)	45
Initial temperature (℃)	20

PCM Property (RT 30)	Value
Melting temperature (℃)	27.7-35
Latent heat capacity (kJ/kg)	206
Thermal conductivity (W/(m · K))	0.18 (solid)
	0.19 (liquid)
Specific heat capacity (kJ/(kg · K))	1.8 (solid)
	2.4 (liquid)

Density (kg/m^3)	789 (solid)
	750 (liquid)

The temperature of point 9 in the PCM domain [43], with the radial position of 27mm and axial position of 650mm, was chosen from the experiment for the validation. As shown in Fig. 5 (a), the numerical results of the temperature varying with time in the first two hours fit well with the experimental results from Trp's work. It should be noted that the effective specific capacity method applied in this study showed more reasonable results, compared with the numerical method adopted by Trp, indicating the importance of considering the temperature range for the phase change process. Fig. 5 (b) shows temperature contours at three different stages (881s, 3674s, 6318s) during the melting process. The effects of mesh size (axial size of 10mm, 5mm and radial size of 0.5mm, 0.25mm) and time step (0.1s, 0.05s) were checked in the validation. The time step of 0.1s, the axial grid size of 10mm and the radial grid size of 0.5mm was finally chosen for the validation shown in Fig. 5. The pressure, velocity and temperature of HTF were validated by the analytical solutions for laminar flows.

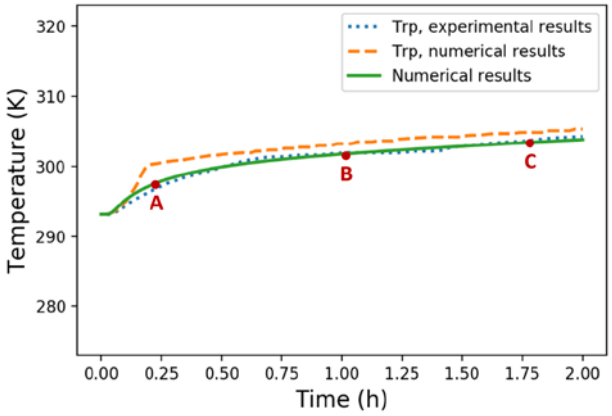

(a) Temperature validation of point 9 in Trp's experiment [43]

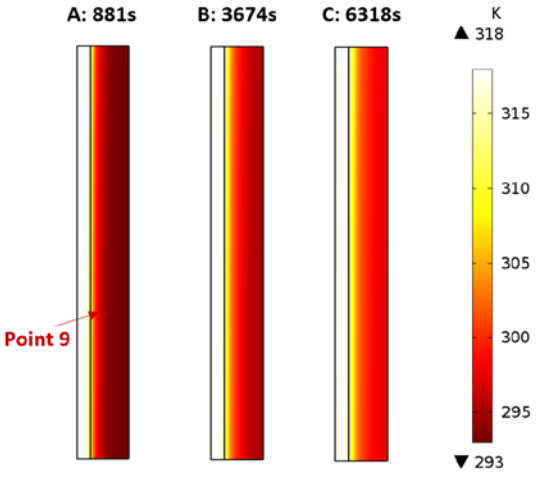

(b) Temperature contours at different stages of melting

Fig. 5. Validation results and temperature contours

2.4 The setting of parametric studies

The default setting for studying the effects of geometric parameters and effective thermal conductivity and the following design optimization were specified as follows. The initial temperature for both HTF and PCM was set as $T_0 = 284\mathrm{K}$. The inlet temperature and inlet velocity of HTF were set as: $T_{in} = 290\mathrm{K}$, $u_{in} = 0.2\mathrm{m/s}$. The properties of the phase change materials are listed in Table 1. The default built-in material of liquid water in the software was applied for HTF, whose properties are dependent on the temperature. The melting temperature range of PCM was set as $\Delta T = 2\mathrm{K}$ in this study, which depends on the type of PCM and the heating/cooling rate.

The heat transfer effectiveness was chosen to be $\eta = 0.8$ and accordingly, the outlet temperature was specified as $T_{out} = 286K$. In other words, when the outlet temperature T_{out} reached $286K$, the simulation would stop. The Parametric Sweep setting in COMSOL was used to complete the numerical simulation in batch.

The geometric parameters of $L = 3\mathrm{m}, d_i = 5\mathrm{mm}, d_o = 10\mathrm{mm}$ were chosen for the independence study on mesh and time step. The result of the mass-weighted average outlet temperature varying with time is shown in Fig. 6. The legends in Fig. 6 show the time step, axial grid size and radial grid size, respectively. Eventually, the axial grid size of 5cm, the radial grid size of 0.1mm, and a time step of 0.02s were set for parametric studies.

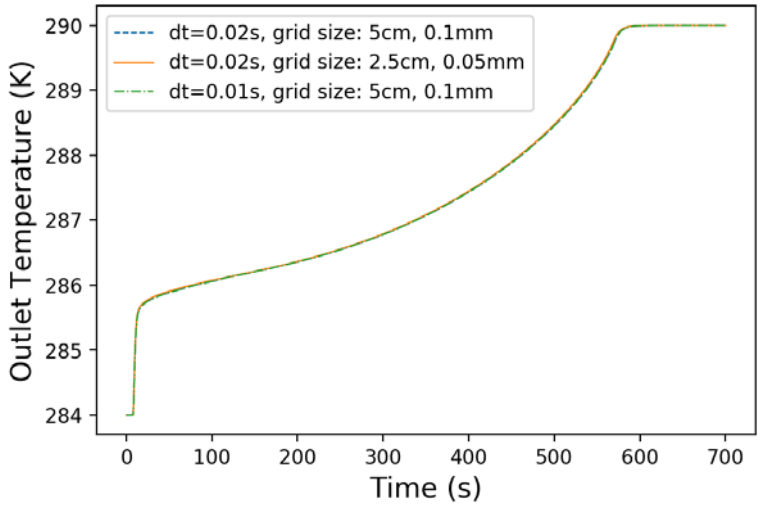

Fig. 6. Mesh and time step sensitivity study

3. Results and Analysis

3.1 The effect of tube length-diameter ratio L/d_i

The effects of geometric parameters for a shell-and-tube type concentric cylinder unit, including tube length L, inner tube diameter d_i and outer tube diameter d_o, were investigated. The thermal conductivity was selected as $k_{\text{eff}} = 4\text{W}/(\text{m}\cdot\text{K})$ in this section.

3.1.1 Tube length

A set of tube lengths was chosen for 20 parametric studies: from 1m to 20m, with an interval of 1m. The outer tube diameter and inner tube diameter were set as $d_o = 10\text{mm}$, $d_i = 5\text{mm}$. The effects of tube length on the outlet temperature T_{out} and the effective energy storage ratio E_{st} are shown in Fig. 7.

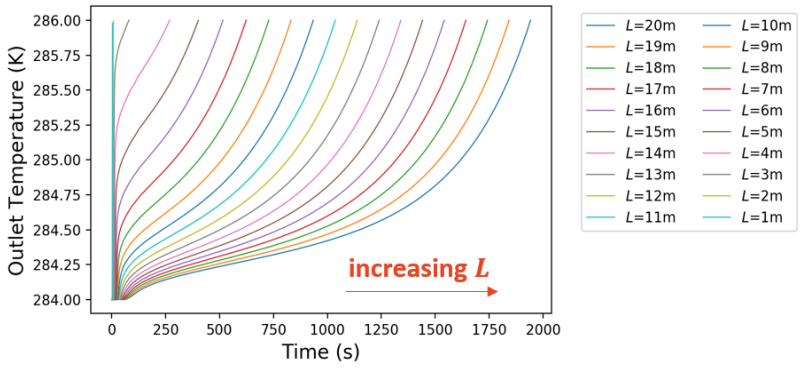

a)

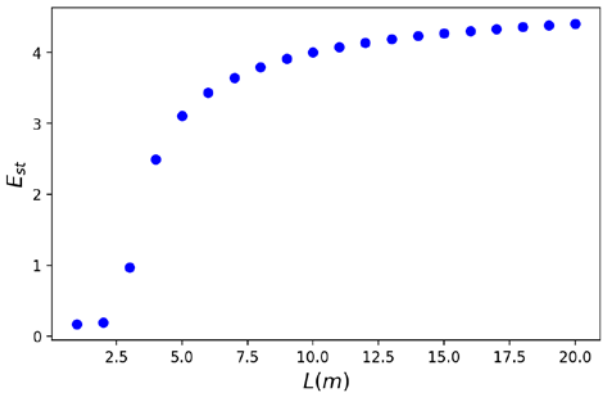

b)

Fig. 7. a) The effect of tube length L on T_{out}; b) The effect of tube length L on E_{st}, with $\text{Re} = 995$, $k_{\text{eff}} = 4\text{W}/(\text{m}\cdot\text{K})$, fixed λ and d_i.

Fig. 7 a) shows that as the tube length increases, the time when T_{out} reaches the specified value increases. It can be observed from Fig. 7 b) that with the increase of the tube length, the effective energy storage ratio E_{st} increases. In other words, the

energy storage system shows better energy storage performance when the tube is longer. The rise of E_{st} may be caused by more complete heat transfer between HTF and PCM, as the heat transfer area enlarges when the tube is longer.

It should be noted that the increasing rate of E_{st} decreases after $L = 4\mathrm{m}$ in Fig. 7 b). Even though the tube length doubles by increasing from $10\mathrm{m}$ to $20\mathrm{m}$, E_{st} only increases by 10%. It means that increasing tube length won't lead to a significant increase in E_{st}, since the speed of the increase slows down. If a higher value of E_{st} is expected, an optimal value of PCM volume ratio λ could be considered, which is analyzed in section 4.3. Moreover, a higher value of the effective thermal conductivity k_{eff} is also recommended.

The numerical results show the benefit of a long tube in a shell-and-tube LHTES unit, in terms of effective energy storage. However, when the tube length is larger, the pressure drop and the energy consumption of the pump are higher. Therefore, it is necessary to consider the energy consumption due to pressure loss. For laminar flow, considering only major loss in pipe flow, the energy consumption of the pump would be as follows [44]:

$$Q_{pump} = \Delta p \dot{V} t = \left(\rho \frac{64}{Re} \frac{L}{d_i} \frac{\bar{u}^2}{2}\right) \dot{V} t \tag{28}$$

The value of Q_{pump}/Q_{eff} in percentage varying with the tube length, which represents the proportion of pump energy consumption in the effective energy storage capacity, is shown in Fig. 8. The percentage increases approximately linearly with the tube length. However, even for $L = 20\mathrm{m}$, Q_{pump} only accounts for 0.022%, which means that the pump energy consumption is negligible when compared with the effective energy storage capacity Q_{eff}.

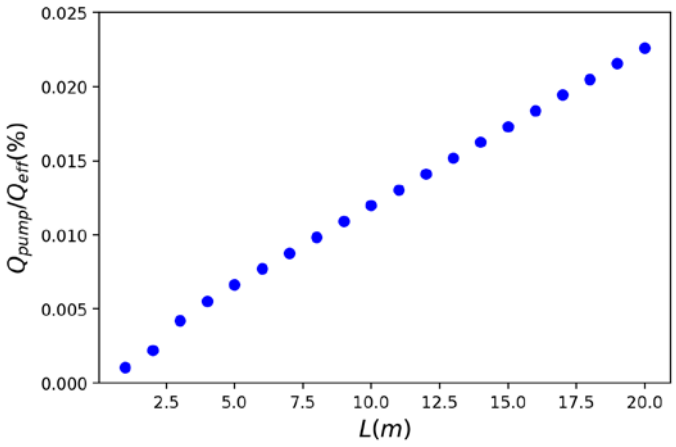

Fig. 8. The proportion of Q_{pump} in Q_{eff} versus tube length, with $\mathrm{Re} = 995$, $k_{eff} = 4\mathrm{W/(m \cdot K)}$, fixed λ and d_i

Meanwhile, the production energy also increases with the increase of tube length. Embodied energy considers the total primary energy consumed to produce the

materials [45], which is applicable to measure the TES system. In this study, it was assumed that the LHTES unit uses the copper tube for HTF transportation and heat conduction. The thickness and density of the copper tube were assumed to be $1\mathrm{mm}$ and $8960\mathrm{kg/m^3}$. After adopting the average embodied energy of copper (50% recycled) as $55.00\mathrm{MJ/kg}$ [45], the embodied energy for a specified tube length $Q_{embodied}$ can be calculated. The energy payback cycle is defined as:

$$n_{cycle} = \frac{Q_{embodied}}{Q_{eff}} \tag{29}$$

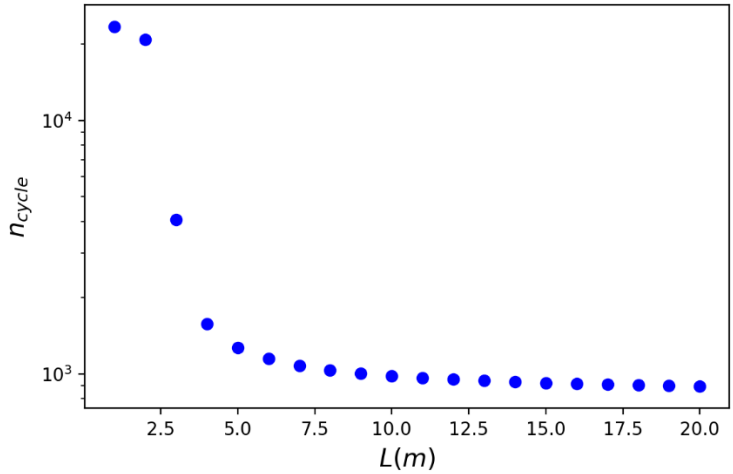

Fig. 9. Energy payback cycle versus tube length, with $\mathrm{Re} = 995$, $k_{\mathrm{eff}} = 4\mathrm{W/(m \cdot K)}$, fixed λ and d_i

The effect of tube length on the energy payback cycle is shown in Fig. 9. The energy payback cycle decreases with the increase of tube length. In other words, the energy investment in the system material can be paid off earlier for units with a longer tube. It should be pointed out that the energy payback cycle n_{cycle} reduces sharply when the tube length increases from $1\mathrm{m}$ to $4\mathrm{m}$ and no significant difference in n_{cycle} can be observed when the tube length is larger than $4\mathrm{m}$. Therefore, a minimum value of the tube length should be ensured for a proper low value of the energy payback cycle n_{cycle}.

In summary, considering that the pump energy consumption is negligible compared with the energy stored, a higher tube length/diameter ratio is always beneficial to improving the energy storage performance of the system, in terms of both effective energy storage ratio E_{st} and energy payback cycle n_{cycle}. As the index E_{st} already considers the total volume of the system V, it can be concluded that a tube-in-tank system with shell-and-tube units configured in series is better than the one configured in parallel. In the meantime, a minimum tube length should be determined to ensure an effective high E_{st} and low n_{cycle} during the design process.

3.1.2 Inner tube diameter

The inner tube diameter d_i is closely related to the flow condition of HTF and is worth investigating. To study the effect of inner tube diameter on the energy storage effectiveness, 9 parametric studies with d_i varying from 2mm to 10mm were performed. The effective thermal conductivity was kept as $k_{\text{eff}} = 4\text{W}/(\text{m}\cdot\text{K})$. The outer tube diameter was $d_o = 12\text{mm}$ and the tube length was $L = 5\text{m}$. The effects of the inner tube diameter d_i on the outlet temperature T_{out} and the effective energy storage ratio E_{st} are shown in Fig. 10.

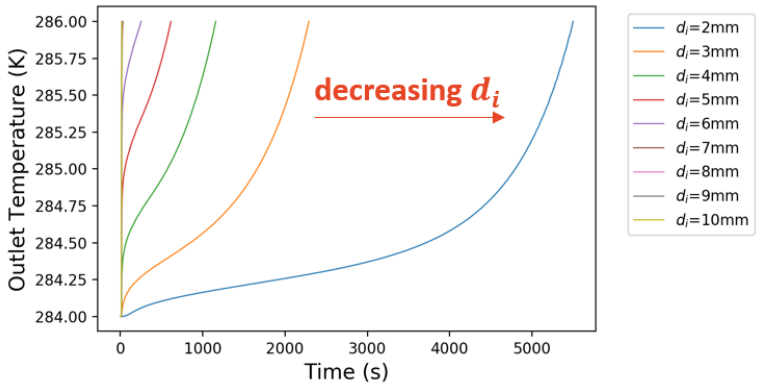

a)

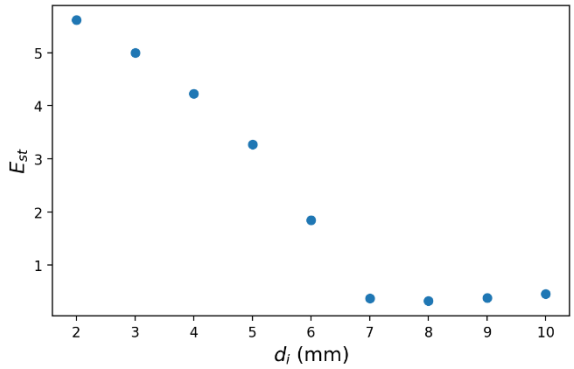

b)

Fig. 10. a) The effect of the inner tube diameter d_i on T_{out}; b) The effect of the inner tube diameter d_i on E_{st}, with $\text{Re} = 995$, $k_{\text{eff}} = 4\text{W}/(\text{m}\cdot\text{K})$, fixed λ and L

Fig. 10 a) shows that as the inner tube diameter drops, the time when T_{out} reaches the specified value increased. It could be observed from Fig. 10 (b) that when the inner tube diameter $d_i > 6\text{mm}$, the effective energy storage ratio $E_{st} < 1$, which means that the energy storage is ineffective. When the energy storage is effective, i.e. $E_{st} > 1$, as the inner tube diameter reduces, the effective energy storage ratio increases, indicating a more effective LHTES system. This is because as the flow rate drops with decreasing inner tube diameter, HTF flowing into the tube could discharge more heat to PCM before it flows out of the tube, which plays a vital role in the increase of the effective energy storage ratio E_{st}. The pressure loss of pipe does not

vary with the inner tube diameter, according to the equation (28) in section 3.1.1, when other parameters are kept the same. Therefore, smaller inner tube diameter is more advantageous to the energy storage effectiveness for the LHTES unit.

3.2 PCM volume ratio

As defined in section 2, PCM volume ratio indicates the proportion of PCM volume in the shell-and-tube LHTES unit. In this work, by changing the outer tube diameter d_o while keeping the inner tube diameter as constant, PCM volume ratio shows how the PCM layer thickness affects the energy storage effectiveness in a shell-and-tube unit. To explore the impact of PCM volume ratio, 17 parametric studies were performed, by adopting the following values of outer tube diameter d_o: 5.5mm, 6mm, 6.5mm, 7mm, 7.5mm, 8mm, 8.5mm, 9mm, 9.5mm, 10mm, 12mm, 14mm, 16mm, 18mm, 20mm, 22mm, 24mm. The according values of PCM volume ratio λ varies from 0.17 to 0.96. The effective thermal conductivity was kept the same as $k_{\text{eff}} = 4\text{W}/(\text{m}\cdot\text{K})$. The inner tube diameter was $d_o = 5\text{mm}$ and the tube length was $L = 5\text{m}$. The effects of the PCM volume ratio on the outlet temperature T_{out} and the effective energy storage ratio E_{st} are shown in Fig. 11.

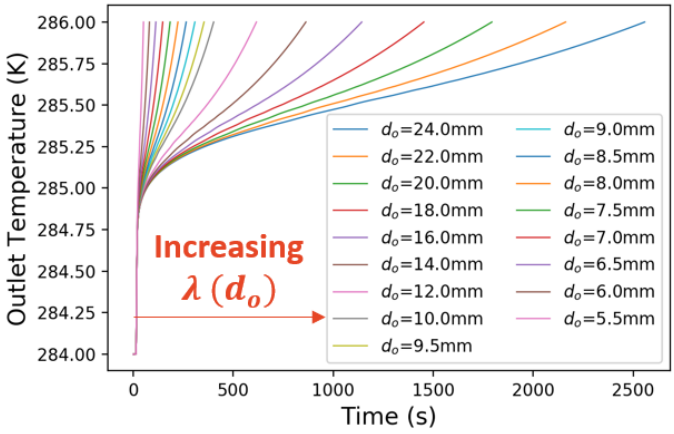

a)

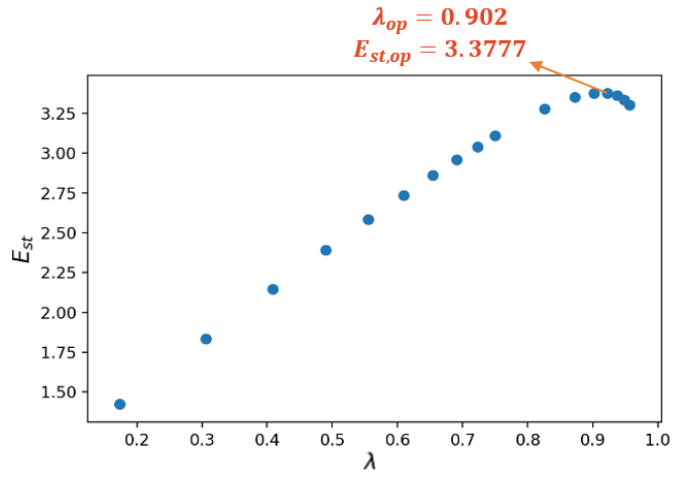

b)

Fig. 11. a) The effect of PCM volume ratio λ on T_{out}; b) The effect of PCM volume ratio λ on E_{st}, with $\mathrm{Re} = 995$, $k_{\mathrm{eff}} = 4\mathrm{W/(m \cdot K)}$, fixed L/d_i

Fig. 11 shows that as the PCM volume ratio increases, the time when T_{out} reaches the specified value increases. However, as PCM volume ratio increases, the effective energy storage ratio E_{st} increases at the beginning and drops afterward. In other words, an optimal PCM volume ratio exists, when the effective energy storage ratio reaches the maximum value. The maximal value of the effective energy storage ratio $E_{st,op} = 3.3777$ is achieved when the optimal PCM volume ratio is $\lambda_{op} = 0.902$. The appearance of optimal PCM volume ratio λ_{op} could be explained by the fact that when λ is small, the amount of PCM is small, which leads to relatively low energy storage capacity. In such case, the potential thermal energy in HTF couldn't be extracted thoroughly by PCM and thus a certain amount of heat is wasted by flowing out the tube directly, rather than being absorbed by PCM. On the other hand, when λ is above a certain threshold, even though the PCM amount is larger, the PCM layer thickness also increases, which results in higher thermal resistance. Therefore, the heat transfer between HTF and PCM is ineffective for a high value of PCM volume ratio, i.e. thick PCM layer. The conclusion that an optimal PCM volume ratio λ_{op} exists, is consistent with Fang et al.'s study [28]. Thus, it is meaningful to investigate how λ_{op} varies under different circumstances, for indicating guidance on practical designs.

3.3 Fixed PCM volume

In this section, the impacts of varying tube length and outer tube diameter on the effective energy storage ratio E_{st}, while the PCM volume is fixed, is investigated. The inner tube diameter is fixed at 5mm. When the tube length is 5m and the outer tube diameter is 10mm, the PCM volume is 2.95e-4m^3, which is adopted as the fixed volume. Consequently, as the tube length increases to 7m or decreases to 3m, the outer tube diameter accordingly decreases to 9mm and increases to 12mm.

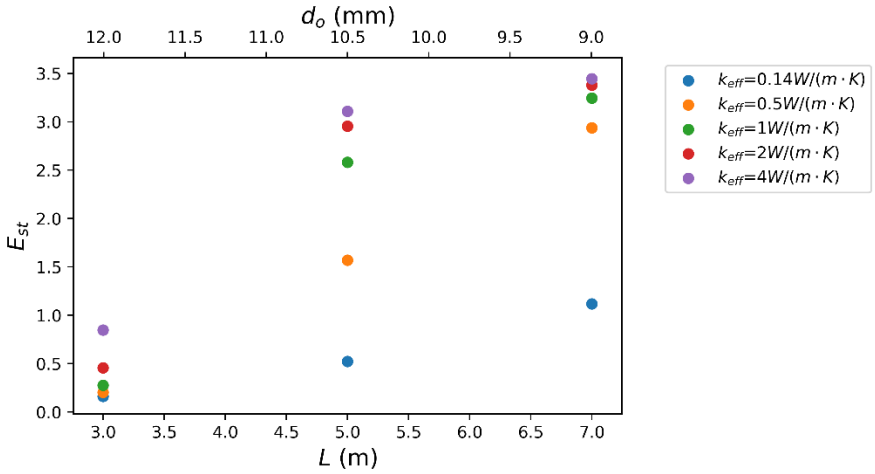

Fig. 12 The effects of tube length L and outer tube diameter d_o on E_{st}, with fixed PCM volume, $\mathrm{Re} = 995$

As shown in Fig. 12, when the PCM volume is fixed, a higher tube length would result in a higher effective energy storage ratio. This could be explained by the fact that a larger heat transfer area exists for a longer tube, which leads to more effective heat transfer between PCM and HTF. Thus, increasing tube lengths is always beneficial to enhance the effective energy storage performance, while it is not true for increasing outer tube diameters, i.e. PCM volume ratios. This is consistent with the conclusion drawn in section 3.1 and 3.2, which puts emphasis on the importance of optimizing the PCM volume ratio to maximize the LHTES system energy storage performance.

3.4 Optimization Analysis

The analysis of the effect of geometric parameters indicates the importance of choosing a long and thin tube for a shell-and-tube unit. More importantly, an optimal PCM volume ratio λ should be determined to maximize E_{st} and ensure the most effective energy storage performance of the shell-and-tube LHTES unit. Therefore, a design optimization guideline is provided by investigating the optimal PCM volume ratio λ_{op} under different geometric parameters of the TES unit and effective thermal conductivity, for laminar and turbulent flow.

In the design optimization, the effects of tube length L and inner tube diameter d_i were considered in one dimensionless index: tube length-diameter ratio L/d_i. The effective energy storage ratio E_{st} increases as L/d_i increases. Over 500 sets of parametric studies for laminar and turbulent flow were performed and the optimal PCM volume ratio λ_{op} was found by maximizing E_{st}. The plots of optimal PCM volume ratio λ_{op} and maximal effective energy storage ratio $E_{st,op}$ versus L/d_i under different k_{eff} are exhibited.

According to studies on the heat transfer enhancement of PCM, the effective thermal conductivity after enhancement with material additives or encapsulation is mainly 0.5-4$\mathrm{W/(m \cdot K)}$ [46]. Even though higher effective thermal conductivity of 10-50$\mathrm{W/(m \cdot K)}$ [6, 7, 47] could possibly be achieved, depending on the material additives type and parameters of the composite, more common values of the effective thermal conductivity k_{eff} were mainly investigated in this study: 0.14$\mathrm{W/(m \cdot K)}$ (pure PCM), 0.5$\mathrm{W/(m \cdot K)}$, 1$\mathrm{W/(m \cdot K)}$, 2$\mathrm{W/(m \cdot K)}$, 4$\mathrm{W/(m \cdot K)}$. An additional set of $k_{\mathrm{eff}} = 20\mathrm{W/(m \cdot K)}$ was applied for the comparison purpose.

3.4.1 Laminar flow

The design optimization of the laminar flow was based upon the settings mentioned in section 3.3. The inner tube diameter $d_i = 5\mathrm{mm}$ was adopted as constant throughout the following studies. The tube length was chosen to be: $L = 3\mathrm{m},\ 4\mathrm{m},$

5m, 6m, 7m and 8m. The Reynolds number $\mathrm{Re} = 995$ is estimated according to below settings: $u_{in} = 0.2\mathrm{m/s}$, $\mu_w = 0.001003\mathrm{kg/(m \cdot s)}$, $\rho_w = 998.2\mathrm{kg/m^3}$. The outer tube diameter $d_o = 6\mathrm{m}$, 6.5m, 7m, 8m, 9m, 10m, 12m, 14m and 18m, keeping the PCM volume ratio λ varying from 0.31 to 0.92. The according value of the tube length-diameter ratio L/d_i varied from 600 to 1600. All combinations of the above parameters were numerically performed and the results of 270 parametric studies in total are discussed.

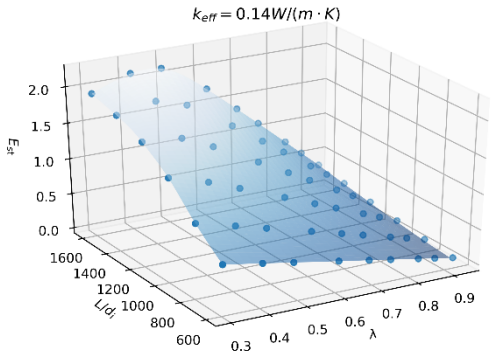

(a) $k_{\mathrm{eff}} = 0.14\mathrm{W/(m \cdot K)}$

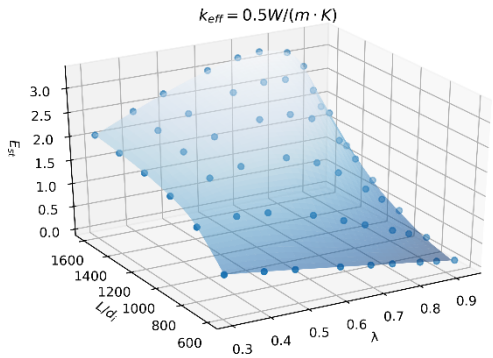

(b) $k_{\mathrm{eff}} = 0.5\mathrm{W/(m \cdot K)}$

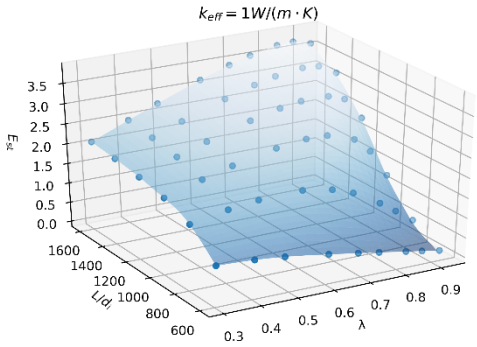

(c) $k_{\mathrm{eff}} = 1\mathrm{W/(m \cdot K)}$

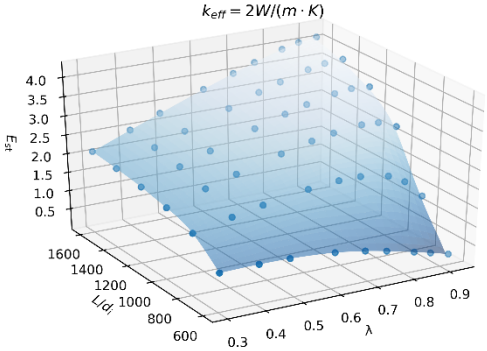

(d) $k_{\mathrm{eff}} = 2\mathrm{W/(m \cdot K)}$

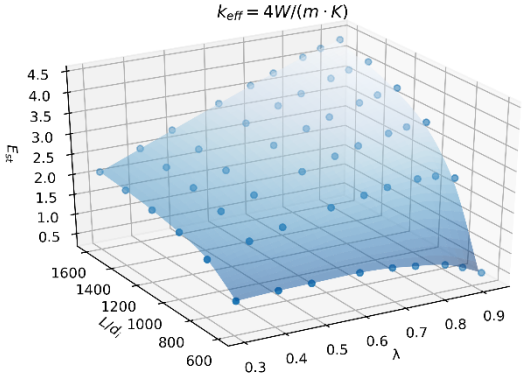

(e) $k_{\mathrm{eff}} = 4\mathrm{W/(m \cdot K)}$

Fig. 13. The effective energy storage ratio E_{st} versus PCM volume ratio λ and tube length-diameter ratio L/d_i under different effective thermal conductivity k_{eff}, with $\mathrm{Re} = 995$

Fig. 13. shows the effective energy storage ratio E_{st} varying with PCM volume ratio λ and tube length-diameter ratio L/d_i under different effective thermal conductivity k_{eff}. It is clearly shown that the trend of E_{st} with varying λ and L/d_i is consistent with the results in section 4. As shown in Fig. 13, a higher value of k_{eff} could noticeably increase the effective energy storage ratio E_{st}. It should be noted that increasing k_{eff} is only effective in enhancing E_{st} when λ is above certain threshold, when L/d_i is fixed. For instance, when $k_{\text{eff}} = 0.14\text{W}/(\text{m}\cdot\text{K})$, E_{st} was limited in the range of 0-2.0 and most of the time the system is ineffective ($E_{st} < 1$). In contrast, for the case of $k_{\text{eff}} = 4\text{W}/(\text{m}\cdot\text{K})$, except when L/d_i is low and λ is high, most cases are effective ($E_{st} > 1$). This can be explained by the fact that under the same geometry, the higher thermal conductivity increases the heat transfer rate between HTF and PCM and thus the energy storage is more effective. Overall, it can be concluded that choosing a higher value k_{eff} is crucial to enhance the effectiveness of the energy storage system.

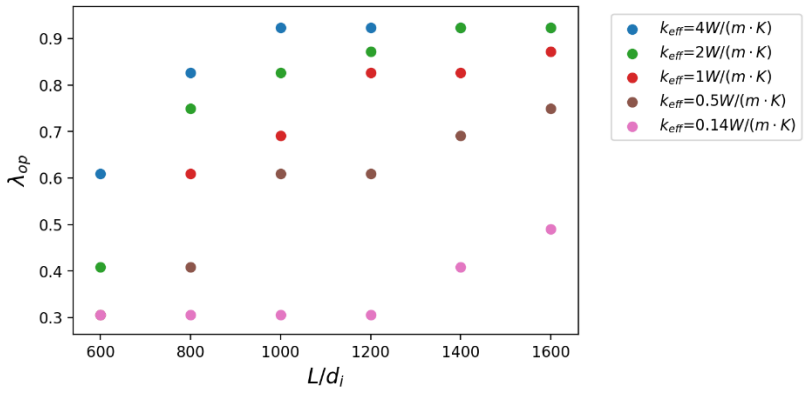

(a) Optimal PCM volume ratio λ_{op}

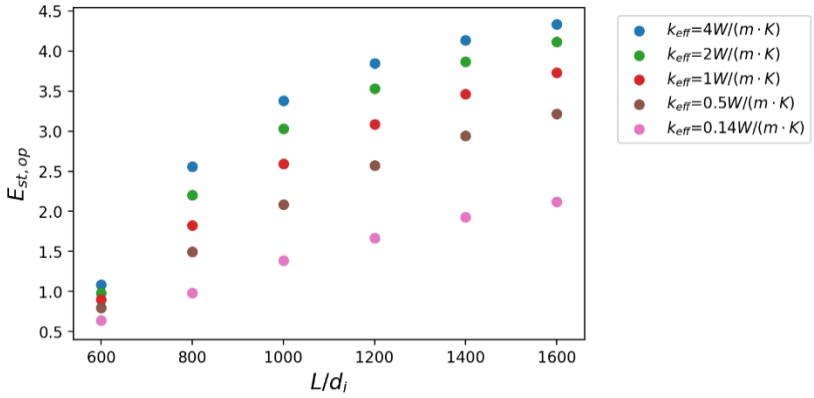

(b) Maximal effective energy storage ratio $E_{st,op}$

Fig. 14. Design optimization of laminar flow ($\text{Re} = 995$)

By picking out the optimal PCM volume ratio case under specific L/d_i and k_{eff} in Fig. 13, a quantitative relationship of optimal PCM volume ratio λ_{op} and maximal effective energy storage ratio $E_{st,op}$ versus L/d_i with varying k_{eff} is summarized in Fig. 14. It can be observed that when either the tube length-diameter ratio L/d_i or effective thermal conductivity k_{eff} is increasing, both λ_{op} and $E_{st,op}$ are increasing.

When longer tube, smaller inner tube or higher effective thermal conductivity are available, the PCM volume ratio should be increased accordingly to ensure the energy storage potential of the LHTES unit with PCM could be fully utilized. The significance of the design optimization figure lies in that it indicates clear quantitative guidance for the designer to choose a proper PCM layer thickness for the shell-and-tube. Even though it is demonstrated that higher k_{eff} would always lead to a more effective energy storage system, it should be also considered that higher k_{eff} could mean using more expensive materials for heat transfer enhancement. Therefore, it is up to the designer to choose a proper approach to enhance the PCM thermal conductivity, as long as the effective energy storage ratio E_{st} is satisfactory for specific applications.

3.4.2 Fully turbulent flow

As for the parametric study setting for turbulent flow, the inner tube diameter $d_i = 22\mathrm{mm}$ was kept as constant. The tube length was selected as $L = 11\mathrm{m},\ 13\mathrm{m},\ 15\mathrm{m},\ 17\mathrm{m},\ 19\mathrm{m},\ 21\mathrm{m}$ and $23\mathrm{m}$, which kept the tube length-diameter ratio L/d_i varying from 500 to 1045. The Reynolds number $\mathrm{Re} = 13134$ is estimated by $u_{in} = 0.6\mathrm{m/s},\ \mu_w = 0.001003\mathrm{kg/(m \cdot s)},\ \rho_w = 998.2\mathrm{kg/m^3}$. Instead of performing all geometric parameter combinations by specifying the outer tube diameter d_o directly, for turbulent flow, the optimal PCM volume ratio λ_{op} was found by keeping d_o as an integer in the unit of millimeter. Accordingly, PCM volume ratio varies from 0.16. Over 150 parametric studies were performed numerically in total. The design optimization results of turbulent flow are shown in Fig. 15.

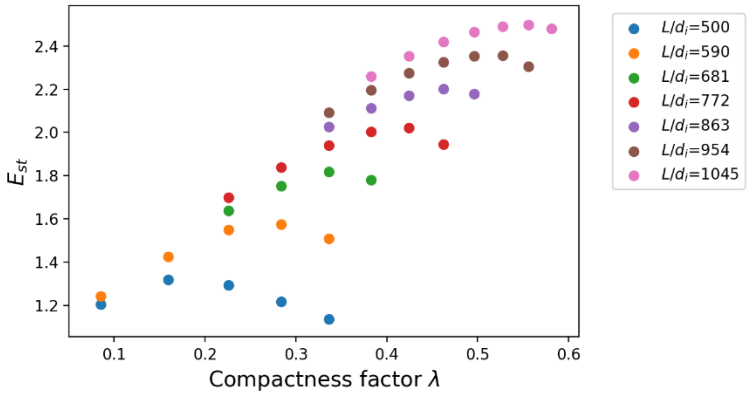

(a) Parametric study results of $k_{\mathrm{eff}} = 4\mathrm{W/(m \cdot K)}$

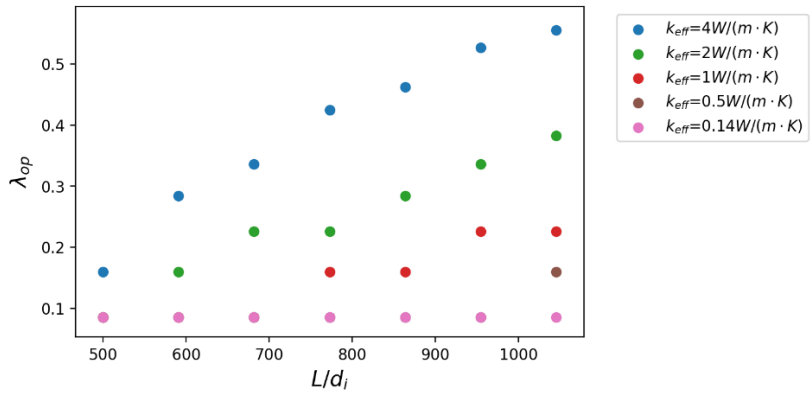

(b) Optimal PCM volume ratio λ_{op}

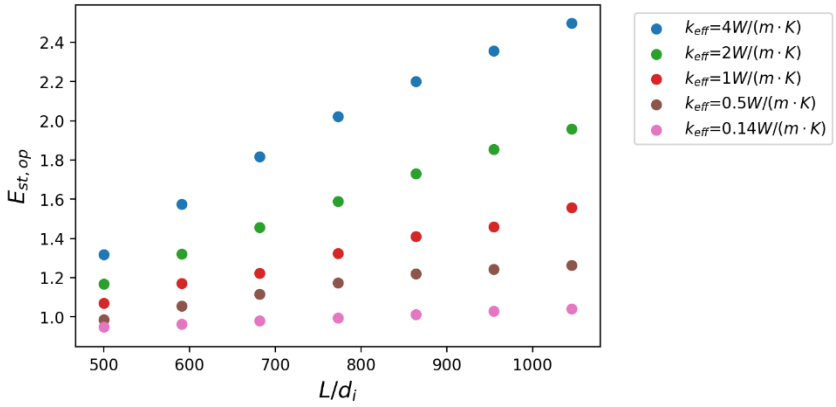

(c) Maximal effective energy storage ratio $E_{st,op}$

Fig. 15. Design optimization of turbulent flow ($\mathrm{Re} = 13134$)

Fig. 15 (a) shows an example of parametric study results when the effective thermal conductivity is $4\mathrm{W/(m \cdot K)}$. As discussed in the laminar flow section, optimal PCM volume ratio λ_{op} also exists for turbulent flow. When PCM volume ratio increases from 0.16, the effective energy storage ratio E_{st} firstly increases and then decreases. By selecting the optimal PCM volume ratio λ_{op} for different L/d_i in the example in Fig. 15 (a), the plot of λ_{op} and the maximal effective energy storage ratio $E_{st,op}$ under different k_{eff} are shown in Fig. 15 (b) and (c), respectively. It could be observed that when Reynolds number is 13134, the TES unit under the optimal PCM volume ratio is effective ($E_{st} > 1$) most of the time, even when L/d_i or k_{eff} is relatively low. $E_{st,op}$ and λ_{op} increases as L/d_i or k_{eff} increases. The results indicate that for higher effective thermal conductivity, PCM thickness should be increased to achieve the optimal PCM volume ratio, which could vary from 0.1-0.6, based on chosen parameters L/d_i. The results provide quantitative guidance towards the design optimization when HTF is turbulent in the pipe, which could serve as a reference for when designing the tube-in-tank LHTES systems.

3.4.3 Comparison

Fig. 16 shows the comparison of design optimization results between the laminar and fully turbulent flow. It is important to point out that laminar flow shows better

energy storage performance than turbulent flow, in terms of the effective energy storage ratio. As shown in Fig. 16 (b), under the same tube length-diameter ratio L/d_i and effective thermal conductivity k_{eff}, the maximal effective energy storage ratio $E_{st,op}$ is generally higher for laminar flow than for turbulent flow, when L/d_i is larger than 800. On the other hand, when L/d_i is around or even smaller than 600, the TES unit with laminar flow is essentially ineffective ($E_{st} < 1$), while turbulent flow could keep the TES unit effective ($E_{st} > 1$). The enhancement of k_{eff} only showed noticeable effects in increasing E_{st} when L/d_i is above a certain threshold: around 800 for laminar flow and around 600 for fully turbulent flow. In short, a TES unit with the long and thin tube, high effective thermal conductivity of PCM and laminar flow for HTF is recommended. Fig. 16 (a) gives guidance on how to choose the optimal PCM volume ratio λ_{op} to ensure the maximum effective energy storage ratio. It should be noticed that the optimal PCM volume ratio λ_{op} of turbulent flow is generally smaller than the one of laminar flow under the same L/d_i and k_{eff}.

The charging rate is mainly determined by the Reynolds number, which is closely related to the flow rate of HTF. As shown in Fig. 16 (c), when the Reynolds number is 13134, i.e. turbulent flow, the charging rate is between 4000W and 6000W. In contrast, the charging rate remains below 100W for laminar flow when the Reynolds number is 995, which is significantly lower. This is because when Reynolds number is higher, the flow rate of HTF is accordingly higher, which leads to faster heat transfer between HTF and PCM. Therefore, turbulent flow is helpful in increasing the heat transfer rate. In this work, fully turbulent flow increases the charging rate by 50 times.

Fig. 16 (d) compares the capacity effectiveness φ under optimal PCM volume ratio between the laminar and turbulent flow. Even though no clear pattern could be observed respectively for laminar and turbulent flow, the TES unit with turbulent flow shows more effective capacity utilization in general, under the same L/d_i and k_{eff}. The capacity effectiveness of turbulent flow is always larger than 0.6, while for laminar flow, the capacity effectiveness varies from 0.2 to 0.7, depending on the choice of L/d_i and k_{eff}.

A set of parametric studies when $k_{\mathrm{eff}} = 20\mathrm{W/(m \cdot K)}$ was added for both laminar and fully turbulent flow for comparison. As shown in Fig. 16 (b), when L/d_i is between 500 and 800, the advantage of fully turbulent flow over laminar flow is more significant, when k_{eff} reaches $20\mathrm{W/(m \cdot K)}$. Meanwhile, when L/d_i is over 850, the difference of $E_{st,op}$ between laminar flow and fully turbulent flow becomes smaller. In general, it is more meaningful to increase the effective thermal conductivity k_{eff} to a high value for fully turbulent flow, since the enhancement of $E_{st,op}$ is significant. However, for laminar flow, no obvious enhancement in terms of $E_{st,op}$ can be observed, when k_{eff} increases from $4\mathrm{W/(m \cdot K)}$ to $20\mathrm{W/(m \cdot K)}$.

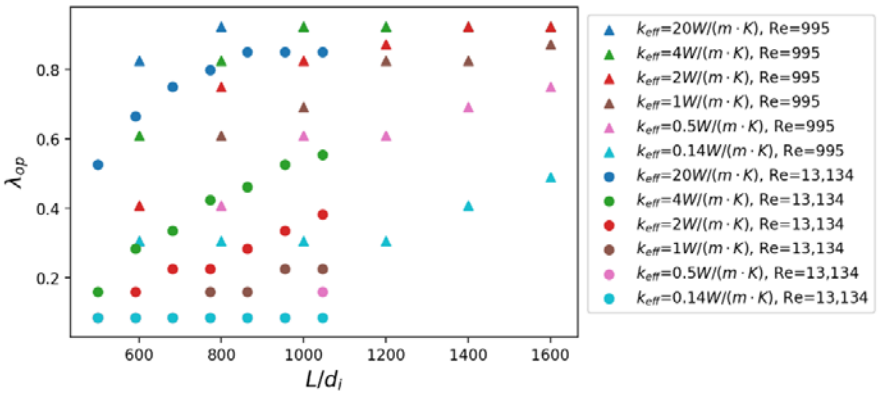

(a) Optimal PCM volume ratio λ_{op}

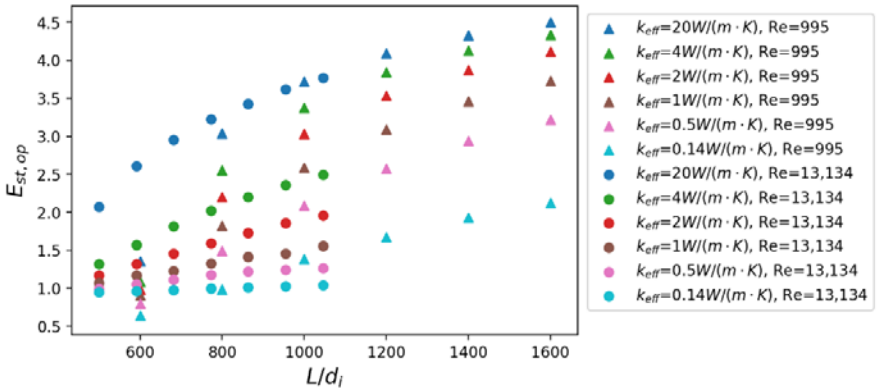

(b) Maximal effective energy storage ratio $E_{st,op}$

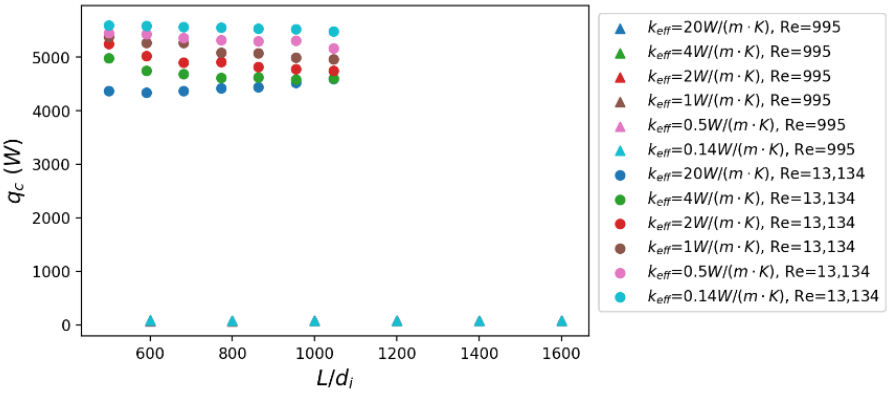

(c) Charging rate q_c

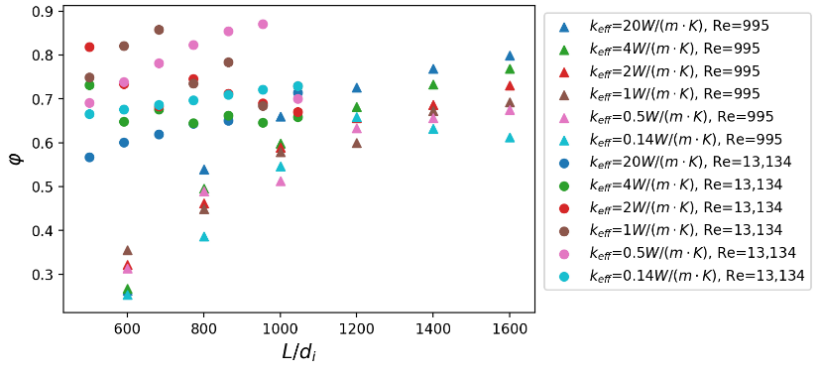

(d) Capacity effectiveness φ

Fig. 16. Optimization comparison between laminar ($\mathrm{Re} = 995$) and fully turbulent flow ($\mathrm{Re} = 13{,}134$)

3.4.4 Low-Re turbulent region

To investigate the energy storage performance when HTF is in the low Reynolds number region, all model settings and parameters were set the same as the ones for fully turbulent flow in section 5.2, except that the inlet velocity of HTF was chosen as 0.2m/s and the tube length was controlled from 9m to 17m. The according Reynolds number is 4379, which is at the beginning of the turbulent region for pipe flow. Over 100 parametric studies were performed for flow in the low-Re turbulent region and the results are shown in Fig. 17.

Unlike the results for HTF in the fully turbulent region, the maximal effective energy storage ratio under optimal PCM volume ratio $E_{st,op}$ of low-Re turbulent flow is higher than the one of laminar flow, under the same L/d_i and k_{eff}, as shown in Fig. 17 (b). This conclusion is worth noticing since it means that turbulent flow is advantageous for the TES unit when the Reynolds number is low, even though a higher Reynolds number would lead to lower E_{st}.

The trend of optimal PCM volume ratio λ_{op} is similar to the one when the Reynolds number is 13,134: as L/d_i or k_{eff} increases, λ_{op} increases. Moreover, the optimal PCM volume ratio of low-Re turbulent flow is generally lower than the one of laminar flow. Higher k_{eff} leads to a lower charging rate at optimal PCM volume ratio for low-Re turbulent flow. The charging rate of the low-Re turbulent flow is from 1400W to 1900W, which is lower than the charging rate of fully turbulent flow. However, it is still around 20 times higher than the charging rate of laminar flow. There is no general trend of capacity effectiveness φ for low-Re turbulent flow. The capacity effectiveness of low-Re turbulent flow is larger than 0.6, which is generally higher than the capacity effectiveness of laminar flow.

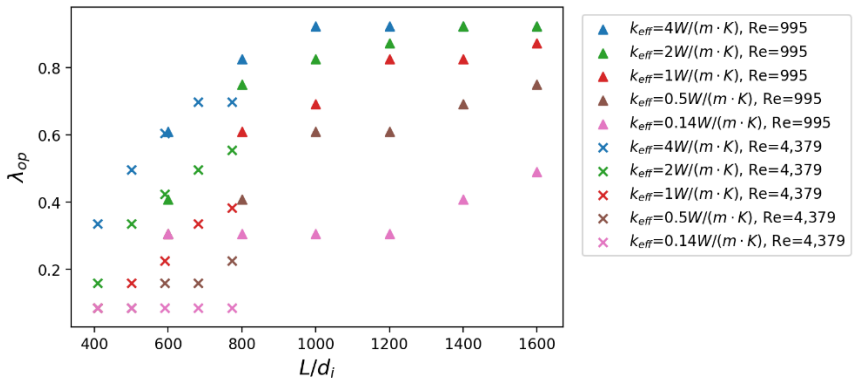

(a) Optimal PCM volume ratio λ_{op}

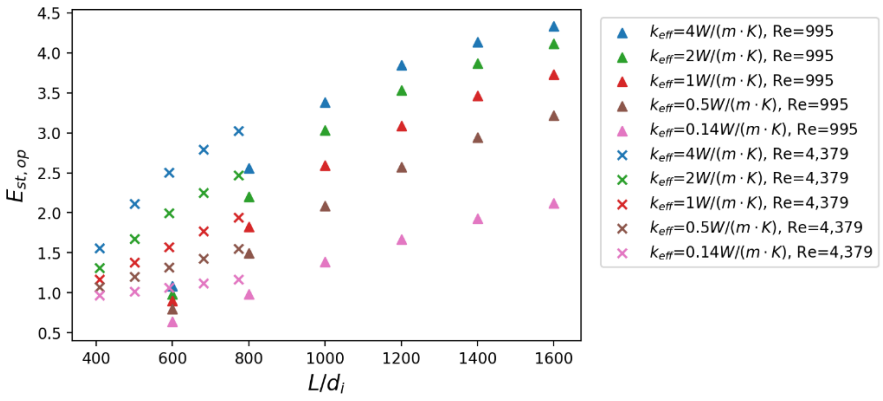

(b) Maximal effective energy storage ratio $E_{st,op}$

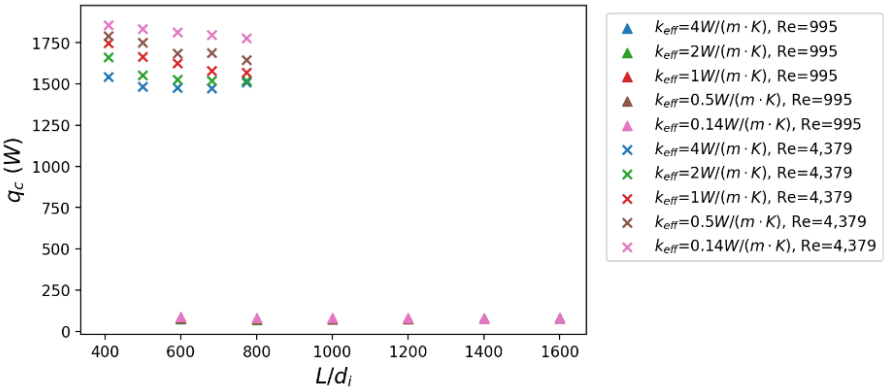

(c) Charging rate q_c

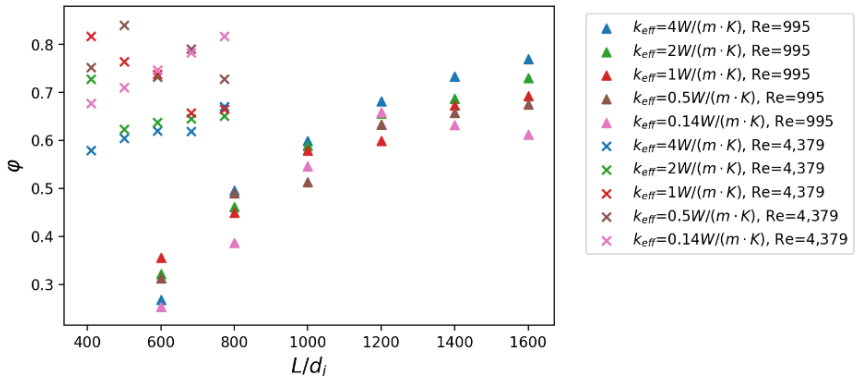

(d) Capacity effectiveness φ

Fig. 17. Optimization comparison between laminar ($\mathrm{Re} = 995$) and low-Re turbulent flow ($\mathrm{Re} = 4{,}379$)

4 Conclusion

This work provides a thorough numerical analysis of the shell-and-tube LHTES device concerning the impacts of design parameters including the tube length-diameter ratio L/d_i, PCM volume ratio λ under various effective thermal conductivities k_{eff} and flow conditions (laminar versus turbulent). Over 500 sets of parametric studies were performed to optimize λ of the shell-and-tube LHTES unit by maximizing E_{st}.

The design optimization for both laminar and turbulent flow was developed as guidance.

- The results of impacts of design parameters show that as tube length-diameter ratio L/d_i increases, the effective energy storage ratio E_{st} increases. This is because a higher tube length leads to a larger heat transfer area, while a smaller inner diameter reduces the HTF flow rate, which means that HTF could discharge more heat to PCM before it flows out of the tube.
- E_{st} captures effects from geometric arrangements and leads to an optimal PCM volume ratio λ_{op}. When λ is too small, the storage capacity of PCM is consequently small and thus a certain amount of heat in HTF is wasted by flowing out the tube directly. However, if λ is too large, the thermal resistance of PCM would be large enough to hinder the effective heat transfer and the PCM far from the inner tube shows ineffective energy storage. Therefore, an optimal PCM volume ratio exists and it is important to optimize λ to achieve the best energy storage performance.
- Increasing k_{eff} is only effective in enhancing E_{st} when λ is above a certain threshold, when L/d_i is fixed.
- The design optimization process optimizes λ by maximizing E_{st}, which gives the optimal PCM volume ratio λ_{op} and the maximal effective energy storage ratio $E_{st,op}$. It is shown that as L/d_i or k_{eff} increases, $E_{st,op}$ and λ_{op} increases.
- Laminar flows ($\mathrm{Re} = 995$) generally show higher $E_{st,op}$, than fully turbulent flows ($\mathrm{Re} = 13134$), under the same L/d_i and k_{eff}. In summary, an LHTES unit with a long and small tube, high effective thermal conductivity of PCM and laminar flow for HTF is recommended.
- With fully turbulent flow, the charging rate q_c can be 50 times higher, and the capacity effectiveness φ under λ_{op} can reach 0.6-0.9 from 0.2-0.8 at laminar flow conditions.
- The enhancement of k_{eff} only noticeably increases $E_{st,op}$ when L/d_i is above a certain threshold, i.e., around 800 for laminar flow and around 600 for fully turbulent flow.
- Significant enhancement in $E_{st,op}$ could be observed when k_{eff} increases from $4\mathrm{W/(m\cdot K)}$ to $20\mathrm{W/(m\cdot K)}$ for fully turbulent flow. Therefore, increasing the effective thermal conductivity to a higher value is recommended for fully turbulent flow. This is because when the effective PCM thermal conductivity is $4\mathrm{W/(m\cdot K)}$ for laminar flow, $E_{st,op}$ is reaching the limit, i.e. the theoretical effective energy storage ratio Q_∞/Q_{SWS}. Less energy storage potential could be extracted for laminar flow when increasing k_{eff} after $4\mathrm{W/(m\cdot K)}$.

It is worth mentioning that HTF in the low-Re turbulent region shows both higher $E_{st,op}$ and charging rate q_c than laminar flow. Considering that the numerical simulation of pipe flow near the flow transition region may not be precise enough, further studies in the low-Re turbulence transition region by experiments would be meaningful. Moreover, the performance index E_{st}, based on effectiveness-NTU theory, can be extended to benchmarking different LHTES systems, and the proposed optimization framework can be a basis for a standard engineering design method.

Declarations of interest: none

References

[1] BP Energy Outlook 2019. BP Energy, 2019.

[2] Renewable Power Generation Costs in 2018. International Renewable Energy Agency (IRENA), 2019.

[3] Nazir H., et al., Recent developments in phase change materials for energy storage applications: A review. International Journal of Heat and Mass Transfer, 2019. **129**: p. 491-523.

[4] Zalba B., et al., Review on thermal energy storage with phase change: materials, heat transfer analysis and applications. Applied Thermal Engineering, 2003. **23**(3): p. 251-283.

[5] Khan Z., Khan Z., and Ghafoor A., A review of performance enhancement of PCM based latent heat storage system within the context of materials, thermal stability and compatibility. Energy Conversion and Management, 2016. **115**: p. 132-158.

[6] Mills A., et al., Thermal conductivity enhancement of phase change materials using a graphite matrix. Applied Thermal Engineering, 2006. **26**(14): p. 1652-1661.

[7] Nomura T., et al., High thermal conductivity phase change composite with percolating carbon fiber network. Applied Energy, 2015. **154**: p. 678-685.

[8] Ling Z., et al., Thermal conductivity of an organic phase change material/expanded graphite composite across the phase change temperature range and a novel thermal conductivity model. Energy Conversion and Management, 2015. **102**: p. 202-208.

[9] He M., et al., Preparation, thermal characterization and examination of phase change materials (PCMs) enhanced by carbon-based nanoparticles for solar thermal energy storage. Journal of Energy Storage, 2019. **25**: p. 100874.

[10] Thapa S., et al., Fabrication and analysis of small-scale thermal energy storage with conductivity enhancement. Energy Conversion and Management, 2014. **79**: p. 161-170.

[11] Li Z. and Wu Z.-G., Numerical study on the thermal behavior of phase change materials (PCMs) embedded in porous metal matrix. Solar Energy, 2014. **99**: p. 172-184.

[12] Al-Jethelah M., et al., Charging nanoparticle enhanced bio-based PCM in open cell metallic foams: An experimental investigation. Applied Thermal Engineering, 2019. **148**: p. 1029-1042.

[13] Zhang Y., Wang X., and Wu D., Microencapsulation of n-dodecane into zirconia shell doped with rare earth: Design and synthesis of bifunctional microcapsules for photoluminescence enhancement and thermal energy storage. Energy, 2016. **97**: p. 113-126.

[14] Rathod M.K. and Banerjee J., Thermal performance enhancement of shell and tube Latent

Heat Storage Unit using longitudinal fins. Applied Thermal Engineering, 2015. **75**: p. 1084-1092.
[15] Aly K.A., El-Lathy A.R., and Fouad M.A., Enhancement of solidification rate of latent heat thermal energy storage using corrugated fins. Journal of Energy Storage, 2019. **24**: p. 100785.
[16] Abdulateef A.M., et al., A combination of fins-nanoparticle for enhancing the discharging of phase-change material used for liquid desiccant air conditioning unite. Journal of Energy Storage, 2019. **24**: p. 100784.
[17] Singh R.P., Kaushik S.C., and Rakshit D., Melting phenomenon in a finned thermal storage system with graphene nano-plates for medium temperature applications. Energy Conversion and Management, 2018. **163**: p. 86-99.
[18] Agyenim F., et al., A review of materials, heat transfer and phase change problem formulation for latent heat thermal energy storage systems (LHTESS). Renewable & Sustainable Energy Reviews, 2010. **14**(2): p. 615-628.
[19] Esen M., Durmuş A., and Durmuş A., Geometric design of solar-aided latent heat store depending on various parameters and phase change materials. Solar Energy, 1998. **62**(1): p. 19-28.
[20] Vyshak N.R. and Jilani G., Numerical analysis of latent heat thermal energy storage system. Energy Conversion and Management, 2007. **48**(7): p. 2161-2168.
[21] Akgün M., Aydın O., and Kaygusuz K., Experimental study on melting/solidification characteristics of a paraffin as PCM. Energy Conversion and Management, 2007. **48**(2): p. 669-678.
[22] Seddegh S., Wang X., and Henderson A.D., A comparative study of thermal behaviour of a horizontal and vertical shell-and-tube energy storage using phase change materials. Applied Thermal Engineering, 2016. **93**: p. 348-358.
[23] Li Y.Q., et al., Numerical analysis and parameters optimization of shell-and-tube heat storage unit using three phase change materials. Renewable Energy, 2013. **59**: p. 92-99.
[24] Lacroix M., Numerical simulation of a shell-and-tube latent heat thermal energy storage unit. Solar Energy, 1993. **50**(4): p. 357-367.
[25] Amin N.A.M., et al., Optimising PCM thermal storage systems for maximum energy storage effectiveness. Solar Energy, 2012. **86**(9): p. 2263-2272.
[26] Youssef W., Ge Y.T., and Tassou S.A., CFD modelling development and experimental validation of a phase change material (PCM) heat exchanger with spiral-wired tubes. Energy Conversion and Management, 2018. **157**: p. 498-510.
[27] Wang W., Wang L., and He Y., The energy efficiency ratio of heat storage in one shell-and-one tube phase change thermal energy storage unit. Applied Energy, 2015. **138**: p. 169-182.
[28] Fang Y., Niu J., and Deng S., Numerical analysis for maximizing effective storage capacity of thermal energy storage systems by enhancing heat transfer in PCM. 2017.
[29] Fang Y., Niu J., and Deng S., An analytical technique for the optimal designs of tube-in-tank thermal energy storage systems using PCM. International Journal of Heat and Mass Transfer, 2019. **128**: p. 849-859.
[30] El Qarnia H., Numerical analysis of a coupled solar collector latent heat storage unit using various phase change materials for heating the water. Energy Conversion and Management, 2009. **50**(2): p. 247-254.
[31] Talmatsky E. and Kribus A., PCM storage for solar DHW: An unfulfilled promise? Solar Energy,

2008. **82**(10): p. 861-869.
[32] Belusko M., Halawa E., and Bruno F., Characterising PCM thermal storage systems using the effectiveness-NTU approach. International Journal of Heat and Mass Transfer, 2012. **55**(13): p. 3359-3365.
[33] Tay N.H.S., Belusko M., and Bruno F., An effectiveness-NTU technique for characterising tube-in-tank phase change thermal energy storage systems. Applied Energy, 2012. **91**(1): p. 309-319.
[34] Lorente S., Bejan A., and Niu J., Phase change heat storage in an enclosure with vertical pipe in the center. International Journal of Heat and Mass Transfer, 2014. **72**: p. 329-335.
[35] Poirier D. and Salcudean M., On Numerical Methods Used in Mathematical Modeling of Phase Change in Liquid Metals. Journal of Heat Transfer, 1988. **110**(3): p. 562-570.
[36] Iten M., Liu S., and Shukla A., Experimental validation of an air-PCM storage unit comparing the effective heat capacity and enthalpy methods through CFD simulations. Energy, 2018. **155**: p. 495-503.
[37] Bo H., Gustafsson E.M., and Setterwall F., Tetradecane and hexadecane binary mixtures as phase change materials (PCMs) for cool storage in district cooling systems. Energy, 1999. **24**(12): p. 1015-1028.
[38] COMSOL Multiphysics 5.3a Documentation.
[39] Incropera F.P., et al., *Fundamentals of heat and mass transfer*. 2007: Wiley.
[40] White F., *Fluid mechanics*. 2003: McGraw-Hill.
[41] Bryant D.B., Sparrow E.M., and Gorman J.M., Turbulent pipe flow in the presence of centerline velocity overshoot and wall-shear undershoot. International Journal of Thermal Sciences, 2018. **125**: p. 218-230.
[42] Kays W.M., *Convective heat and mass transfer*. 2012: Tata McGraw-Hill Education.
[43] Trp A., An experimental and numerical investigation of heat transfer during technical grade paraffin melting and solidification in a shell-and-tube latent thermal energy storage unit. Solar energy, 2005. **79**(6): p. 648-660.
[44] Pritchard P.J., Mitchell J.W., and Leylegian J.C., *Fox and McDonald's Introduction to Fluid Mechanics, Binder Ready Version*. 2016: John Wiley & Sons.
[45] Hammond G., et al., *Inventory of carbon & energy: ICE*. Vol. 5. 2008: Sustainable Energy Research Team, Department of Mechanical Engineering.
[46] Lin Y., et al., Review on thermal conductivity enhancement, thermal properties and applications of phase change materials in thermal energy storage. Renewable and Sustainable Energy Reviews, 2018. **82**: p. 2730-2742.
[47] Wang Z., et al., Paraffin and paraffin/aluminum foam composite phase change material heat storage experimental study based on thermal management of Li-ion battery. Applied Thermal Engineering, 2015. **78**: p. 428-436.